ARTICLE

Highly Effective Detection of Amitraz in Honey by Using Surface-Enhanced Raman Scattering Spectroscopy Coupled with Chemometric Methods

Xin-ming Nie[a], Jing Wang[b], Xun Wang[a], Ya-ping Tian[c], Si Chen[a], Zhou-yang Long[b*], Cheng-hua Zong[b*]

a. School of Physics and Electronic Engineering, Jiangsu Normal University, Xuzhou 221116, China
b. School of Chemistry and Materials Science, Jiangsu Key Laboratory of Green Synthesis for Functional Materials, Jiangsu Normal University, Xuzhou 221116, China,
c. Kewen College, Jiangsu normal university, Xuzhou 221116, China

(Dated: Received on August 27, 2018; Accepted on October 22, 2018)

As an effective and universal acaricide, amitraz is widely used on beehives against varroasis caused by the mite *Varroa jacobsoni*. Its residues in honey pose a great danger to human health. In this study, a sensitive, rapid, and environmentally friendly surface-enhanced Raman spectroscopy method (SERS) was developed for the determination of trace amount of amitraz in honey with the use of silver nanorod (AgNR) array substrate. The AgNR array substrate fabricated by an oblique angle deposition technique exhibited an excellent SERS activity with an enhancement factor of $\sim 10^7$. Density function theory was employed to assign the characteristic peak of amitraz. The detection of amitraz was further explored and amitraz in honey at concentrations as low as 0.08 mg/kg can be identified. Specifically, partial least square regression analysis was employed to correlate the SERS spectra in full-wavelength with C_{amitraz} to afford a multiple-quantitative amitraz predicting model. Preliminary results show that the predicted concentrations of amitraz in honey samples are in good agreement with their real concentrations. Compared with the conventional univariate quantitative model based on single peak's intensity, the proposed multiple-quantitative predicting model integrates all the characteristic peaks of amitraz, thus offering an improved detecting accuracy and anti-interference ability.

Key words: Amitraz, surface-enhanced Raman spectroscopy method, Oblique angle deposition, Honey, Detection, Sensing, Ag nanorod, Density function theory, Partial least squares regression

I. INTRODUCTION

Amitraz is a formamidine pesticide widely used in agriculture and veterinary medicine as insecticide and acaricide. Specifically, it is one of the most effective pesticides against Varroa destructor, a mite parasite, which endangers beekeeping all over the world [1]. However, amitraz can suppress the central nerve and the respiratory system by reacting with α-2-adrenergic receptor, causing serious human poisoning. Because of this, the use of amitraz was banned in United States since 2005 [2]. Unfortunately, a large amount of amitraz is still used in the remainder countries due to its efficacy and low price. For this reason, maximum residues limits (0.2 mg/kg) are in force all over the world [3].

Currently, the most widely used methods for amitraz detection are high performance liquid chromatography (HPLC) [4], gas chromatography-electron capture detection (GC-ECD) [5], gas chromatography with mass spectrometry (GC-MS) [6], high performance liquid chromatography with mass spectrometry (HPLC-MS) [7]. Although these methods have high sensitivity, ideal repeatability, they usually require long analysis time, complicated procedures, and significant special skills. In this regard, establishing a simple and cost-effective detection method for reliable detection of amitraz in honey is still in great need.

Surface-enhanced Raman spectroscopy (SERS), as a powerful and extremely sensitive analytical technique, has been well employed for detecting analytes at very low concentrations [8−14]. Particularly, it produces a narrow band spectral signature unique to the molecular vibrations of the analyte, which can effectively avoid the matrix interference and provide the most promising advantages in complex sample detection. The key to perform a SERS experiment is the choice and/or fabrication of the noble-metal substrate since the performance of SERS depends strongly on the localized surface plasmon resonance (LSPR) properties of the nano-

*Authors to whom correspondence should be addressed. E-mail: longzhouyangfat@163.com, zongch@jsnu.edu.cn

structured metal [15−18]. Thus far, various nanostructures fabricated by different techniques have been explored to manifest the SERS effect, such as vapor deposition [19, 20], colloidal lithography [21, 22], and e-beam lithography [23, 24]. These substrates exhibit excellent SERS performance, most are, however, either expensive or time-consuming, and fail to fabricate reproducible substrates in large scale. In this context, oblique angle deposition (OAD) has emerged as a promising alternative [25−27]. By varying the deposition conditions, the size, shape and density of the nanostructures can be easily controlled, which open up a new avenue in constructing high performance SERS substrates for sensing applications [28]. Despite these great advantages, it remains a great challenge for using SERS to accurately detect analytes in complex samples as most of the current available SERS detecting methods are operated by correlating the concentration of the analytes with their single characteristic peak's intensity [29−31]. Although these univariate quantitative models are advantageous in terms of simplicity, they suffer from low anti-interference ability.

With this in mind, herein a multiple-quantitative amitraz detecting model was proposed by coupling partial least square regression (PLSR) analysis with SERS method based on Ag nanorod (AgNR) arrays substrates. The AgNR arrays were prepared by using OAD technique, which exhibits excellent sensitivity and reproducibility. Density functional theory (DFT) was performed to confirm the characteristic peaks and corresponding vibrational modes of amitraz. In this case, a univariate quantitative model was firstly established by correlating the characteristic peak area of amitraz with its concentration. Finally, to make the detection more robust, a multiple-quantitative amitraz predicating model was constructed by correlating the SERS spectra of amitraz in full-wavelength with its concentration through PLSR analysis. Different from conventional univariate quantitative method based on single characteristic peak' intensity, this multiple-quantitative model integrates all the characteristic parameters of amitraz, and therefore it is expected to offer improved detecting accuracy and anti-interference ability, which holds great promise for real applications.

II. MATERIALS AND METHODS

A. Materials

Amitraz (2-methyl-1,3-di (2,4-xylylimino)-2-azapropane) was purchased from Sigma Chemical Co., Ltd. (USA). *Trans*-1,2-bis (4-pyridyl) ethylene (BPE) was acquired from J&K China Chemical Ltd. (China) Silver (99.999%) and titanium (99.995%) pellets were purchased from Kurt J. Lesker Co., Ltd. (USA). *n*-Hexane was acquired from Sinopharm Chemical Reagent Co., Ltd. (China). Honey sample was purchased from a local supermarket (Xuzhou, China). Ultra-pure water ($\geq$18.2 MΩ) was used in all experiments.

B. Fabrication of AgNR array substrates

The AgNR array substrate is prepared by OAD method in an electron beam deposition system (DE500, DE Technology Inc., Beijing, China). 1 cm×1 cm glass slides were sonicated in ethanol solution for 10 min and dried in high purity nitrogen, then were loaded into the deposition chamber. The deposition began as the chamber pressure reached 5×10^{-7} torr. 20 nm of titanium films and 100 nm silver films were deposited on glass substrate at the rate of 0.2 nm/s and 0.3 nm/s, respectively. In order to ensure the smoothness of the film, these films were deposited at an incident angle θ=0° relative to the normal of the substrate. Then, the substrate was rotated to an oblique angle of θ=86° with respect to the vapor incident direction (FIG. 1 (a, b)). The quartz crystal microbalance (QCM d) was used to monitor sedimentary thickness and sedimentation rate. The deposition process stopped at a QCM reading of 2 μm.

C. Sample preparation

Different concentrations of amitraz (0.1, 0.4, 1, 2, 3, 5, 10, 20, 30, 50, and 100 mg/L) were prepared by solving *n*-hexane to determine the SERS intensity versus C_{amitraz} calibration curve and the LOD. BPE (1×10^{-6} mol/L) solution was used to determine the SERS enhancement factor of the Ag NR array. Furthermore, practical applications of the sensing platform in monitoring amitraz in honey were accomplished as follows: 25 g of the honey samples spiked with amitraz were dissolved in 40 mL ultrapure water, and then 10 mL of the resulted solution was mixed with 10 mL *n*-hexane for amitraz extraction. This step was repeated for three times and the supernatant was concentrated to a final concentration of 5 mL, afterwards, the obtained solution was dropped onto the AgNR array for SERS detection as demonstrated in FIG. 1(c).

D. SERS measurement

The Raman analyzer (ProRaman-L-785A2, Enwave Optronics, Irvine, CA) equipped with a 785 nm diode laser (85 μm diameter), was used to perform all the SERS measurements. The Raman analyzer includes a spectrometer and an integrated fiber optic Raman probe for excitation and signal collection through a 10× objective lens. 2 μL of sample was added to the AgNR array substrate each time, and dried under the same ambient conditions. The integration time is 10 s with a laser power of 30 mW. In order to ensure the credibility of detection, at least seven random sampling spots were collected each well.

DOI:10.1063/1674-0068/cjcp1808193

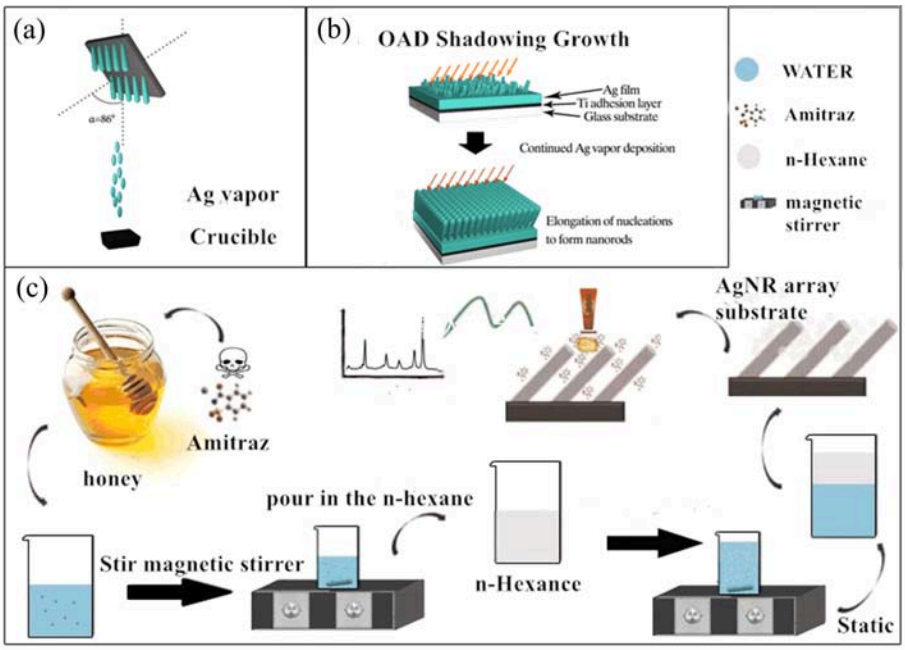

FIG. 1 (a) Schematic diagram of the AgNR substrate fabrication by OAD. (b) The growth process of AgNR array substrates. (c) Sample pretreatment and SERS detection of amitraz in the honey.

E. Spectral data analysis

All SERS spectra were plotted by Origin 8.5 (Origin Lab, Northampton, MA). Spectral analysis was performed using a GRAMS/AI Spectrum Software Kit (Thermo Fisher Scientific, Waltham, MA). Statistical analysis was performed using Matlab 2010a (Mathworks, Denver, CO). 3D structure was constructed by 3D Studio Max 2018(Autodesk). With the help of Gaussian 09W DFT package, the Raman spectra of the amitraz and the corresponding vibrational modes were accurately identified. The DFT calculations were based on Becke's three-parameter exchange function (B3) [32] with the dynamic correlation function of Lee, Yang, and Parr (LYP) [33]. A modest 6-311G(d) basis set of B3LYP function was used to optimize the molecular structure of amitraz [31].

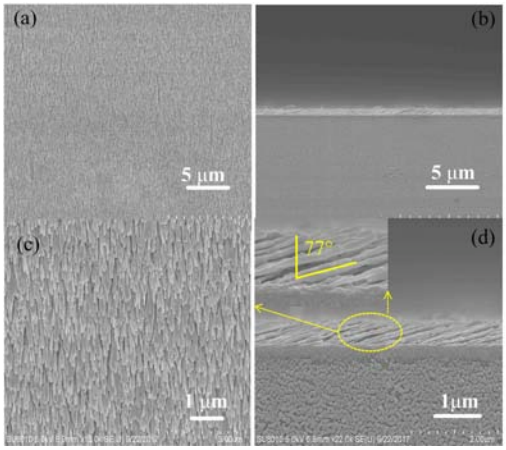

FIG. 2 SEM images of the AgNR array substrate fabricated by OAD at different magnification times (a, c) and their corresponding cross-section SEM images (b, d).

III. RESULTS AND DISCUSSION

A. Fabrication and characterization of AgNR array substrates

The OAD method (FIG. 1(a, b)) was used to prepare the highly sensitive and reproducible substrates, and the top-view and cross-sectional views of the substrates were examined with a scanning electron microscope (FIG. 2). The results exhibit that the AgNR length was about (958±50) nm with a tilting angle of approximately 77° relative to the substrate normal. The diameter of the AgNR and the gap between these rods as shown in the magnified SEM image were (100±30) nm and (110±40) nm, respectively.

According to the literature, the high energy local hot spots of the Ag nanorods were mainly distributed in the angular space between nanorods and silver films and the top of the nanorods. The enhancement ability of the AgNR substrate was estimated by using biological dye molecules BPE (1×10^{-6} mol/L, 2 μL) as probe. As demonstrated in FIG. 3, the peak intensity of the SERS spectrum is significantly stronger than that of the Raman spectrum, and no obvious peaks were observed in the background spectrum. The enhancement factor

DOI:10.1063/1674-0068/cjcp1808193

was calculated as follows [34]:

$$EF = \left(\frac{I_{\mathrm{SERS}}}{I_{\mathrm{Raman}}}\right) \times \left(\frac{N_{\mathrm{Roman}}}{N_{\mathrm{SERS}}}\right) \quad (1)$$

$$N_{\mathrm{SERS}} = C_{\mathrm{SERS}} V_{\mathrm{SERS}} \times \frac{S_{\mathrm{laser}}}{S_{\mathrm{SERS}}} \times N_{\mathrm{A}} \quad (2)$$

$$N_{\mathrm{Raman}} = C_{\mathrm{Raman}} V_{\mathrm{laser}} \times N_{\mathrm{A}} \quad (3)$$

where I_{SERS} (=5×10^3) and I_{Raman} (=350) are the peak intensities of the SERS and Raman spectra at 1200 cm^{-1}, N_{SERS} and N_{Raman} are the number of BPE molecules illuminated by the laser focus spot under SERS and normal Raman conditions. C_{SERS}=1×10^{-6} mol/L and C_{Raman}=1×10^{-2} mol/L are the corresponding concentrations of BPE used in SERS and normal Raman detection. The volume of BPE added to the AgNR array susbtrate was V_{SERS}=2 μL. The solution was spread circularly in a diameter of 2 mm, thus S_{SERS}=πr^2=3.14×10^{-6} m^2; the calculated laser beam area S_{laser}=7.6×10^{-12} m^2 (r=3.1×10^{-6} m) [34]. The volume of the BPE solution producing Raman scattering was calculated to be V_{laser}=2.5×10^{-12} m^3 [34]. N_{A} is avogadro constant (N_{A}=6.02×10^{23}). According to the calculation, the SERS enhancement factor of the Ag nanorod arrays is about 2.2×10^7. To test the uniformity of the AgNR array, the SERS spectra of BPE molecules from 30 randomly spots of an AgNR array substrate were recorded, and the spot-on-spot intensity variation of the characteristic was presented in FIG. S1. According to the statistics of the predominant peak's intensity, the relative standard deviation (RSD) for the band vibrations of BPE at 1200 and 1607 cm^{-1} is 9.1% and 11.2%, respectively. These results revealed clearly that the AgNR array are uniform and capable of generating SERS signals with good reproducibility.

B. SERS peak assignments of amitraz based on DFT calculation

Encouraged by the excellent sensitivity and uniformity of the AgNR array, the substrate was then used for the quantification of amitraz. To that end, DFT was performed to determine the characteristic peaks of amitraz and their corresponding vibrational modes. The theoretical Raman spectrum as calculated by DFT and the SERS spectrum of amitraz as well as the Raman spectrum of the amitraz powder are shown in FIG. 4. Experimentally, the theoretical Raman and the amitraz spectrum show similar characteristic peaks. However, small differences can also be observed because of the base group setting and the experimental conditions. The main typical vibration peaks are located in the spectral region of 720 cm^{-1} to 1668 cm^{-1}, and the vibration peak distribution is determined based on the results of DFT. As shown in Table I, the SERS spectra of amitraz are mainly derived from C=N−C scissoring, C−H rocking, and ring scissoring. According

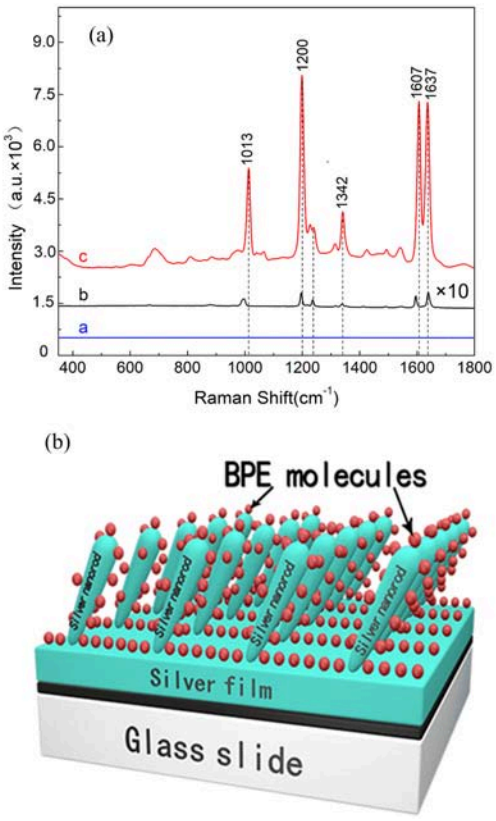

FIG. 3 (a) Background of AgNR array substrate, Raman spectrum of 10^{-2} BPE solution and SERS spectrum of 10^{-6} mol/L BPE solution, (b) 3D simulation schematic diagram of BPE molecules distributed inside AgNR array.

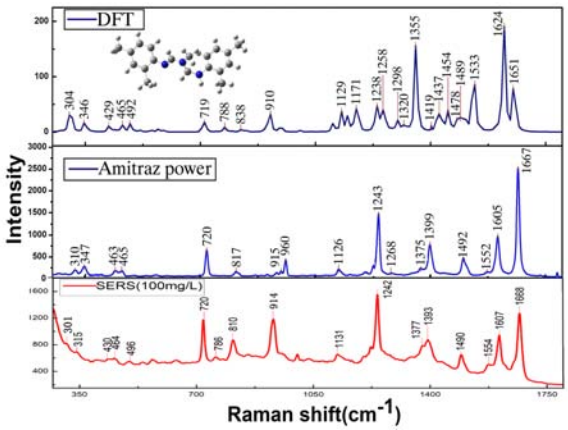

FIG. 4 The Raman spectra calculated by DFT (navy) and the corresponding bulk Raman (blue) and SERS (red) spectra of amitraz.

to the structural characteristics of amitraz molecules, the peaks at 720, 1242, and 1490 cm^{-1} can attribute to the benzene ring vibration, benzene ring breathing vibration, and C−H rocking vibration; while the 1393 and 1668 cm^{-1} are derived from the N=C−H bending vibration, and N=C−N symmetrical stretching vibra-

DOI:10.1063/1674-0068/cjcp1808193

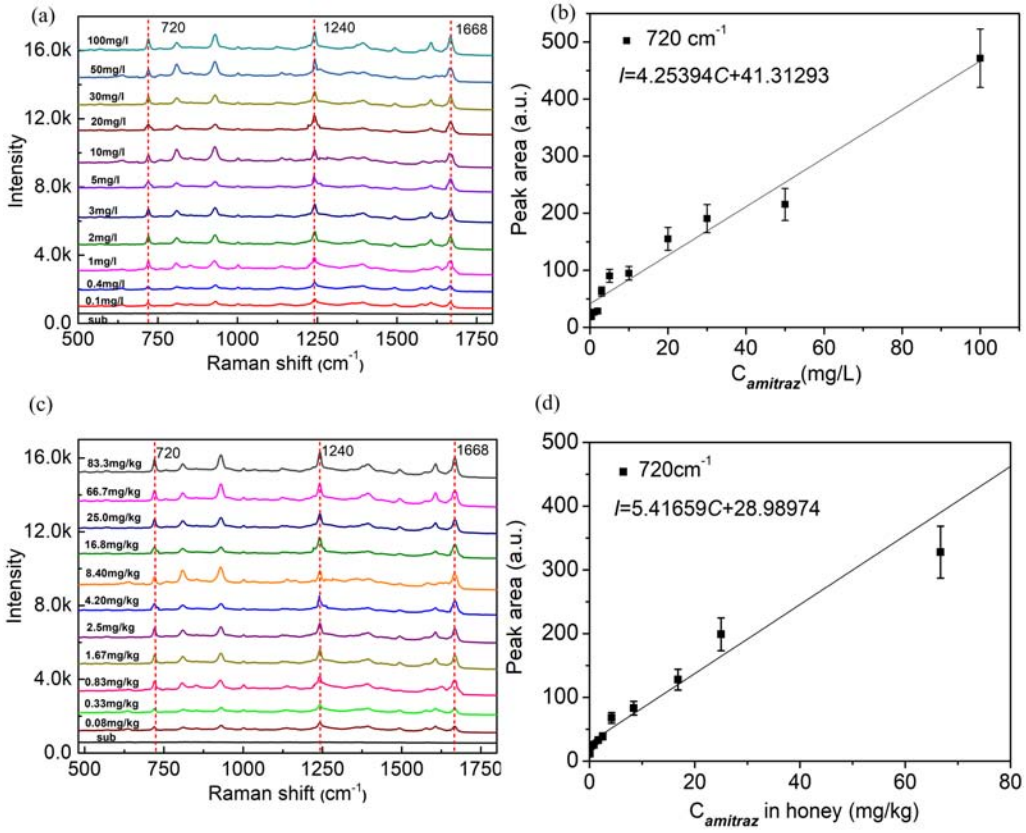

FIG. 5 (a) SERS spectra of the amitraz in *n*-hexane at different concentration, (b) the average (obtained by GRAMS/AI spectroscopy software suite) peak area of characteristic peak 720 cm^{-1} as an LS function of amitraz concentration, (c) the SERS spectra of amitraz extracted from honey samples, (d) the average peak area of the characteristic peak at 720 cm^{-1} as a LS function of the Amitraz concentration in honey.

tion.

C. Detection of the amitraz using the AgNR array substrate

FIG. 5(a) shows the representative SERS spectra of different concentration amitraz in *n*-hexane. Amitraz at concentrations as low as 0.1 mg/L can be well distinguished from the higher resolution and smoothed spectra. To analyze the change in the characteristic SERS peaks quantitatively, a standard procedure, GRAMS/AI spectroscopy software suite was used to fit the spectra. The obtained peak area at 720 cm^{-1} was used to determine the limit of the detection (LOD). FIG. 5(b) reveals the linear curve describing the peak areas as a function of amitraz concentration. A linear dependence was obtained over the range of 0.1−100 mg/L, and the LOD is calculated to be 0.05 mg/L at a signal-to-noise ratio of 3, which clearly validates the sensing performance of the AgNR array substrate toward amitraz.

Encouraged by the above promising results, the AgNR array substrate was further applied to detect amitraz in honey. In proof of concept experiments, the honey samples spiked with different concentration of amitraz were dissolved in water, and then *n*-hexane was added for amitraz extraction. The mixed liquor was dropped on the AgNR array substrates for SERS detection. It took about 5−10 s to stabilize the surface after *n*-hexane evaporation. The SERS spectra of honey sample, *n*-hexane and amitraz are shown in FIG. S2 (supplementary materials). In consistent with amitraz alone, the increase of amitraz in honey affords an increased SERS intensity and a wide linear correlation in a concentration range from 0.08 mg/kg to 83.3 mg/kg (FIG. 5(c, d)). The recoveries of standard addition are 118.7%, 108%, and 82.7% for amitraz concentration of 8.4, 16.8, and 66.7 mg/kg, respectively. These results reveal the practicality of using the present sensing platform for amitraz determination.

D. Repeatability evaluation based on principal component analysis (PCA)

To verify the repeatability of the AgNR substrate toward amitraz detection, PCA, which has proven to be a powerful tool for processing SERS spectra [35−37], was employed to evaluate the measured SERS data in the

DOI:10.1063/1674-0068/cjcp1808193

TABLE I Band assignments for the DFT-Raman, experimental normal Raman, and SERS spectra of amitraz.

Band/cm^{-1}			Assignments
DFT	Raman	SERS	vibrational modes
304	310	303	$C_{25}-H_{27}$ rocking
346	347	350	Ring wagging
429		430	$N_{21}-C_{26}-N_{28}$ scissoring
465	463	464	Ring wagging
492	465	496	Ring scissoring
719	720	720	Ring scissoring
788		786	$C_{32}-H_{35}$ & C_{34}-H_{38} rocking
838	817	810	Ring scissoring
910	915	930	$C_{19}-N_{18}-C_4$ scissoring
1129	1126	1131	Ring scissoring
1171			$C_{32}-C_{34}$ stretching
1238	1241	1242	Ring scissoring+(C−H) formation vibration
1258	1268	1262	Ring scissoring
1298			Ring stretching
1320			Ring scissoring
1355	1375	1377	$C_{35}-H_{17}$ rocking
1419	1399	1393	N=C−H in-plane bending
1437			Ring stretching
1454			$C_{26}-N_{28}$ stretching
1478			$C_{25}-N_{28}$ stretching
1489	1492	1490	C−H formation vibration
1533	1552	1552	$H_{23}-C_{22}$-H_{24} scissoring
1621	1605	1607	$C_{19}-N_{18}$ stretching
1624			Ring scissoring
1651	1667	1668	N=C−N symmetry stretching vibration

full spectrum range. PCA can determine the distribution of different sampling points at the same concentration by scoring each factor in the sample. As shown in FIG. S3 (supplementary materials), after the PCA full spectrum analysis, it was found that the same concentration of sampling point data was gathered together, and only a few points were close to each other because of the proximate concentration. As listed in Table S1 (supplementary materials), when the principal components of them were set to 4, the cumulative contribution rate of PCs is 96.6% and average RSD is 10.42%. Impressively, it was noted that by using PCA full spectrum analysis, amitraz at concentration as low as 0.04 mg/kg can be well distinguished from the blank honey sample; while amitraz at the same concentration cannot be defined confidently in the SERS spectra (not given). This result reveals the great advantages of full-spectrum and multivariate analysis.

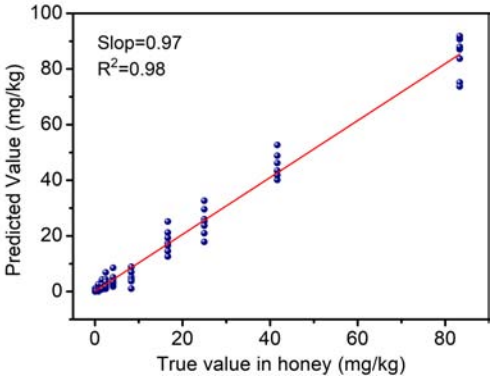

FIG. 6 PLSR analysis of amitraz in honey (each concentration was measured seven times).

E. Linear regression and prediction of amitraz detection based on PLSR

The compositions of real samples are so complex and some peaks of the SERS active component may overlap with the characteristic peak of the analyte, lowering the detection accuracy, and even inducing false positive signals. To make the detection more robust, it is important to analyze the SERS spectra of the analyte in full-wavelength to obtain multivariate correlation parameters. To that end, PLSR was employed to correlate the SERS spectra of amitraz in whole wavelength with C_{amitraz} to afford a multiple-quantitative amitraz predicating model. FIG. 6 is the linear fitting built between the predicted amitraz concentration and its real values. Theoretically, the closer the slope to 1, the more accurate of the prediction is. In this case, the coefficient of determination R^2 is 0.98, suggesting that the calibration curves exhibit a good linear fitting. Moreover, the slopes between the predicted and observed concentrations are 0.97, revealing that the predicted concentrations of the unknown data points are in good agreement with their real concentrations.

IV. CONCLUSION

A fast and highly efficient SERS method for the detection of amitraz residues in honey was developed by using AgNR array substrate. The as-prepared substrate exhibited an excellent performance with a detection limit of 0.08 mg/L, and kept a high reproducibility with a detection variation within 11%. Furthermore, by using PLSR, a multiple-quantitative prediction model was established, which has been used successfully for the prediction of amitraz in honey sample with high accuracy. The superiority of excellent sensitivity, high reproducibility and accuracy as well as the low cost are integrated in the present method, which is very promising in real sample applications.

DOI:10.1063/1674-0068/cjcp1808193

Supplementary materials: SERS spectra of 10^{-6} mol/L BPE taken from 30 random spots on the AgNR substrates (FIG. S1); Raman spectra of honey, *n*-hexane, and the amitraz (FIG. S2); PCA analysis of amitraz with different concentrations extracted from the honey samples (FIG. S3); variance, contribution rate, and cumulative contribution rate of amitraz (Table S1) are available.

V. ACKNOWLEDGMENTS

This work was supported by the Natural Science Foundation of the Higher Education Institutions of Jiangsu Province (No.16KJB510009 and No.17KJB510017), Jiangsu Province Natural Science Foundation of China (BK20150228).

[1] J. J. Jimenez, J. L. Bernal, M. J. del Nozal, and C. Alonso, Anal. Chim. Acta **524**, 271 (2004).
[2] H. Guo, P. Zhang, J. W. Wang, and J. Zheng, J. Chromatogr. B **951**, 89 (2014).
[3] J. Z. Xu, J. J. Miao, H. Lin, T. Ding, Z. Y. Zhao, B. Wu, C. Y. Shen, and Y. Jiang, J. Sep. Sci. **32**, 4020 (2009).
[4] A. C. Martel and S. Zeggane, J. Chromatogr. A **954**, 173 (2002).
[5] J. H Zhou, X. F. Xue, Y. Li, J. Z. Zhang, L. M. Wu, L. Z, Chen, and J. Zhao, J. Sep. Sci. **30**, 1912 (2007).
[6] I. Notardonato, P. Avino, G. Cinellia, and M. V. Russo, Food Anal. Methods **9**, 1675 (2016).
[7] C. Ferrer, A. Agera, M. Mezcua, A. R. Fernández-Alba, D. Mack, M. Anastassiades, and M. Gamón, J. Aoac. Int. **93**, 380 (2010).
[8] D. W. Li, W. L. Zhai, Y. T. Li, and Y. T. Long, Microchim. Acta **181**, 23 (2014).
[9] S. Zou, L. Ma, J. Li, Z. Xie, D. Zhao, Y. Ling, and Z. Zhang, Talanta **186**, 452 (2018).
[10] S. Yang, X. Dai, B. B. Stogin, and T. S. Wong, Proc. Nat. Acad. Sci. USA **113**, 268 (2016).
[11] L. L. Qu, D.W. Li, J.Q. Xue, W. L. Zhai, J. S. Fosseyab, and Y. T. Long, Lab Chip. **12**, 876 (2012).
[12] Z. H. Luo, L. N. Chen, C. J. Liang, Q. M. Wei, Y. Chen, and J. Wang, Microchim. Acta. **184**, 3505 (2017).
[13] T. Senapati, D. Senapati, A. K. Singh, Z. Fan, R. Kanchanapally, and P. C. Ray, Chem. Commun. **47**, 10326 (2011).
[14] S. S. R. Dasary, Y. K. Jones, S. L. Barnes, P. C. Ray, and A. K. Singh, Sens. Actuators B: Chem. **224**, 65 (2016).
[15] R. G. Freeman, K. C. Grabar, K. J. Allison, R. M. Bright, J. A. Davis, A. P. Guthrie, M. B. Hommer, M. A. Jackson, P. C. Smith, and D. G. Walter, Science **267**, 1629 (1995).
[16] K. Liu, Y. Bai, L. Zhang, Z. Yang, Q. Fan, H. Zheng, Y. Yin, and C. Gao, Nano Lett. **16**, 3675 (2016).
[17] S. Z. Oo and M. D. B. Charlton, Opt. Express. **24**, 27425 (2016).
[18] Y. Hirai, H. Yabu, Y. Matsuo, K. Ijirocd, and M. Shimomura, Chem. Commun. **46**, 2298 (2010).
[19] W. D. Ruan, C. X. Wang, N. Ji, W. Xu, and B. Zhao, Chem. J. Chin. U. **28**, 768 (2007).
[20] V. Peksa, P. Lebruskova, H. Sipova, J. Štěpánek, J. Bok, J. Homolab, and M. Procházka, Phys. Chem. Chem. Phys. **18**, 19613 (2016).
[21] A. Hakonen, M. Svedendahl, R. Ogier, Z. J. Yang, K. Lodewijks, R. Verre, T. Shegai, and P. O. Andersson, Nanoscale **7**, 9405 (2015).
[22] N. A. Cinel, S. Cakmakyapan, S. Butun, G. Ertas, and E. Ozbay, Photonic Nanostruct. **15**, 109 (2015).
[23] W. Yue, Z. Wang, X. Wang, L. Q. Chen, Y. Yang, B. Chew, A. Syed, K. C. Wong, and X. X. Zhang, J. Nanosci. Nanotechnol. **12**, 696 (2012).
[24] Y. He and Y. Zhao, Nanoscale **3**, 2361 (2011).
[25] Y. J. Liu, Z. Y. Zhang, Q. Zhao, R. A. Dluhy, and Y. P. Zhao, J. Phys. Chem. C **113**, 9664 (2009).
[26] Q. Zhou, X. Zhang, Y. Huang, Z. Li, Y. P. Zhao, and Z. J. Zhang, Appl. Phys. Lett. **100**, 113101 (2012).
[27] J. D. Driskell, S. Shanmukh, Y. Liu, S. B. Chaney, X. J. Tang, Y. P. Zhao, and R. A. Dluhy, J. Phys. Chem. C. **112**, 895 (2008).
[28] C. Q. Han, J. Chen, X. M. Wu, Y. W. Huang, and Y. P. Zhao, Talanta **128**, 293 (2014).
[29] J. Chen, Y. Huang, P. Kannan, L. Zhang, Z. Lin, J. Zhang, T. Chen, and L. Guo, Anal. Chem. **88**, 2149 (2016).
[30] N. Zhou, G. Meng, Z. Huang, Y. Ke, Q. Zhou, and X. Hu, Analyst **141**, 5864 (2016).
[31] L. L. Qu, Y. Y. Liu, M. K. Liu, G. H. Yang, D. W. Li, and H. T. Li, ACS Appl. Mater. Interfaces **8**, 28180 (2016).
[32] A. D. Becke, J. Chem. Phys. **98**, 5648 (1993).
[33] W. Y. C. Lee and G. R. Parr, Phys. Rev. B **37**, 785 (1988).
[34] B. Giese and D. McNaughton, J. Phys. Chem. B **106**, 101 (2011).
[35] M. Hou, Y. Huang, L. Ma, and Z. Zhang, Nanoscale Res. Lett. **10**, 437 (2015).
[36] S. Zou, M. Hou, J. Li, L. Ma, and Z. Zhang, Sci. Rep. **7**, 6186 (2017).
[37] M. Hou, Y. Huang, L. Ma, and Z. Zhang, Nanoscale Res. Lett. **11**, 296 (2016).

DOI:10.1063/1674-0068/cjcp1808193